JOURNAL OF SYNCHROTRON RADIATION
ISSN 1600-5775

Received 14 March 2019
Accepted 16 May 2019

Edited by R. W. Strange, University of Essex, UK

Keywords: soft X-ray absorption measurements; 3*d* transition metal oxides; thin-film engineering; thickness-dependent properties.

Asymmetric response of electrical conductivity and V valence state to strain in cation-deficient $Sr_{1-y}VO_3$ ultrathin films based on absorption measurements at the V L_2- and L_3-edges

Meng Wu,[a]* Si-Zhao Huang,[b] Hui Zeng,[a] Gertjan Koster,[b] Yu-Yang Huang,[a] Jin-Cheng Zheng[a] and Hui-Qiong Wang[a]*

[a]Fujian Provincial Key Laboratory of Semiconductors and Applications, Collaborative Innovation Center for Optoelectronic Semiconductors and Efficient Devices, Department of Physics, Xiamen University, Xiamen 361005, People's Republic of China, and [b]1 MESA+ Institute for Nanotechnology, University of Twente, Enschede, The Netherlands. *Correspondence e-mail: meng.wu@xmu.edu.cn, hqwang@xmu.edu.cn

The correlation between electronic properties and epitaxial strain in a cation-deficient system has rarely been investigated. Cation-deficient $SrVO_3$ films are taken as a model system to investigate the strain-dependent electrical and electronic properties. Using element- and charge-sensitive soft X-ray absorption, V *L*-edge absorption measurements have been performed for $Sr_{1-y}VO_3$ films of different thicknesses capped with 4 u.c. (unit cell) $SrTiO_3$ layers, showing the coexistence of V^{4+} and V^{5+} in thick films. A different correlation between V valence state and epitaxial strain is observed for $Sr_{1-y}VO_3$ ultrathin films, *i.e.* a variation in V valence state is only observed for tensile-strained films. $Sr_{1-y}VO_3$ thin films are metallic and exhibit a thickness-driven metal–insulator transition at different critical thicknesses for tensile and compressive strains. The asymmetric response of electrical conductivity to strain observed in cation-deficient $Sr_{1-y}VO_3$ films will be beneficial for functional oxide electronic devices.

1. Introduction

Perovskite transition metal oxides show fascinating physical properties attractive for both device applications and theoretical investigations. Among these materials, non-stoichiometry can easily be formed and indeed is one of the crucial parameters in determining the novel properties. For instance, oxygen vacancies provide an excellent platform for tuning the electrical, magnetic and optical properties in titanates (Tarun *et al.*, 2013), manganites (Ma *et al.*, 2016), cobaltates (Stemmer *et al.*, 2001) and iron-based multiferroic compounds (Farokhipoor & Noheda, 2011). The coupling between strain and oxygen vacancies has been emphasized in a review article recently that showed the strongly correlated features in a diversity of perovskite systems which might be beneficial for information and energy technologies (Herklotz *et al.*, 2017). Another form of non-stoichiometry with cation deficiencies and/or an excess of oxygen atoms behaves differently, which can for instance induce a *p*-type conductivity as observed in manganite (Skjarvo *et al.*, 2016), an enhanced T_c and more complicated physics as reported in high-T_c cuprates (Pan *et al.*, 2001), or novel interfacial properties as reported in $LaTiO_{3+\delta}$ and $LaNiO_3$ heterostructures (Cao *et al.*, 2016). However, the correlation between electronic properties and epitaxial strain in a cation-deficient and/or extra oxygen-doped system has rarely been investigated, so this will be addressed in our present study.

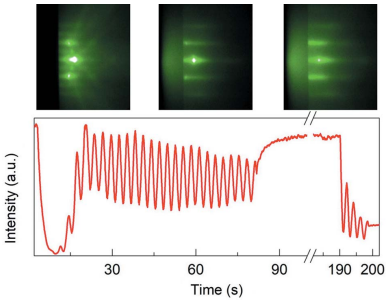

The $SrVO_3$ (SVO) parent compound shows an ideal cubic crystal symmetry of lattice constant 3.843 Å. The correlated SVO thin films exhibit dimension-controlled metallic quantum well structures and a metal–insulator transition below a critical thickness (Yoshimatsu *et al.*, 2011, 2013). The low resistivity of an SVO film as well as the excellent structural and chemical compatibility between SVO and other isostructural compounds show its potential application as the electrode layer for functional perovskite oxide devices (Moyer *et al.*, 2013). However, experimental synthesis meets difficulties in the following aspects. Firstly, the partially filled V 3*d* shell allows a set of different valence states ranging from V^{5+} to V^{2+}, which can form a number of single- and multi-valence vanadium oxides with various physical and spectroscopic properties (Wu *et al.*, 2018; Sawa *et al.*, 2002; Yoshino *et al.*, 2017). Secondly, the oxide ceramic target for SVO film deposition is usually single-phase polycrystalline $Sr_2V_2O_7$ which requires extremely reducing conditions to stabilize V^{4+}. Therefore, non-stoichiometry can easily be created for thin-film engineering related to SVO, similar to another well studied early transition metal compound $LaTiO_3$ using an $La_2Ti_2O_7$ target (Ohtomo *et al.*, 2002). Therefore, the understanding of the electrical properties of SVO thin films deserves particular attention. The easy oxidation of V ions to V^{5+} in SVO films brings the possibility of investigating the interplay between cation deficiency and other degrees of freedom.

In this article, we present a study of the electrical conductivity and valence state of cation-deficient $Sr_{1-y}VO_3$ thin films capped with 4 u.c. (unit cell) $SrTiO_3$ (STO) layers. Different epitaxial strain-dependent studies show an asymmetric correlation between the V valence state and the strain effect in ultrathin $Sr_{1-y}VO_3$ films. We also provide a detailed analysis of the electrical transport properties of the strain- and thickness-dependent $Sr_{1-y}VO_3$ films. Our present studies shed light on understanding the electrical and electronic properties of functional oxides, as well as designing and optimizing functional oxide devices.

2. Experimental methods and results

2.1. Sample deposition and structural characterization

The $Sr_{1-y}VO_3$ thin films were deposited on STO, $LaAlO_3$ (LAO) and $LaSrAlO_4$ (LSAO) substrates by pulsed laser deposition from a single-phase $Sr_2V_2O_7$ polycrystalline target, using a KrF excimer with a laser energy density of 2 mJ cm^{-2} and a frequency of 5 Hz. The temperature was increased at a rate of 10 K min^{-1} and stabilized at 1053 K to prevent surface contamination. An ultrahigh-vacuum pressure of 10^{-8} Torr (1 Torr = 133.322 Pa) is a prerequisite for film deposition in an extremely reducing environment. The materials were deposited at a substrate temperature of 983 K with an Ar flow at a pressure of 2×10^{-2} Torr. A nonreactive Ar atmosphere has been demonstrated as an effective strategy for high-quality SVO thin-film deposition at low oxygen pressure (Wang *et al.*, 2018; Mirjolet *et al.*, 2019), which influences the propagation of the plasma plume through reducing the kinetic energy of the species therein. After film growth, the temperature was lowered at a constant rate of 10 K min^{-1} to room temperature while the pressure was kept unchanged. All the deposited thin films were capped with 4 u.c. STO to prevent the influence of surface oxidation kinetics and interface energies (Ohtomo *et al.*, 2002). The lattice parameters of the substrate and the lattice mismatch are shown in Table 1.

Table 1
Lists of composition, (pseudo-)cubic or tetragonal lattice constants c_{sub} and a_{sub} of the substrate, the lattice mismatch calculated by $(a_{sub} - a_{SVO})/a_{SVO}$ using bulk SVO with a lattice constant $a = b = c = 3.843$ Å, the measured out-of-plane lattice constant of an SVO thin film c_{film}, the measured in-plane lattice constant a_{film} and the relaxation $R = (a_{film}^{meas} - a_{sub})/(a_{film}^{relax} - a_{sub})$, with a_{film}^{meas} and a_{film}^{relax} denoting the in-plane lattice constants of the strained and relaxed layers, respectively.

The lattice parameters for 10 u.c. $Sr_{1-y}VO_3$ on LSAO were not measured due to the measurement limit of a typical in-house XRD setup.

SVO on	c_{sub} (Å)	a_{sub} (Å)	Mismatch (%)	c_{film} (Å)	a_{film} (Å)	R (%)
STO (26 u.c.)	3.905	3.905	1.6	3.846	3.905	0
LAO (26 u.c.)	3.79	3.79	−1.4	3.94	3.822	60
LSAO (10 u.c.)	12.636	3.756				

In situ reflection high-energy electron diffraction (RHEED) is highly surface sensitive and was used to provide real-time monitoring of the film deposition process. The electron diffraction patterns of cation-deficient SVO thin films [Figs. 1(*b*)–1(*c*)] show broadened streaks, indicating a surface of monolayer roughness and a two-dimensional layer-by-layer crystal growth. The growth rate and precise control of the unit-cell thickness were determined from the RHEED oscillations, where each full period oscillation corresponds to the formation of a single atomic layer thickness.

Figs. 2(*a*)–2(*b*) show high-resolution X-ray diffraction scans along the specular direction for a 26 u.c. $Sr_{1-y}VO_3$ film deposited with tensile and compressive strains, respectively. Figs. 2(*c*)–2(*d*) show the corresponding reciprocal-space maps around the 013 reflection. From the read-off positions of the

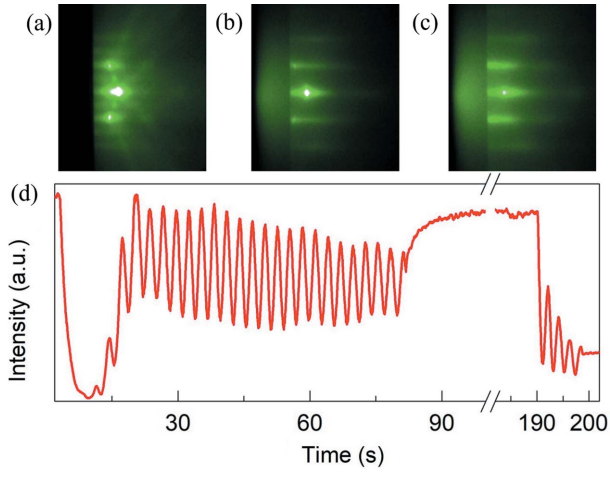

Figure 1
RHEED images captured (*a*) before deposition, (*b*) after $Sr_{1-y}VO_3$ film deposition and (*c*) after deposition of the STO capping layers. (*d*) A RHEED oscillation pattern for a 26 u.c. $Sr_{1-y}VO_3$ film (10 nm) with a 4 u.c. STO capping layer deposited on an STO substrate.

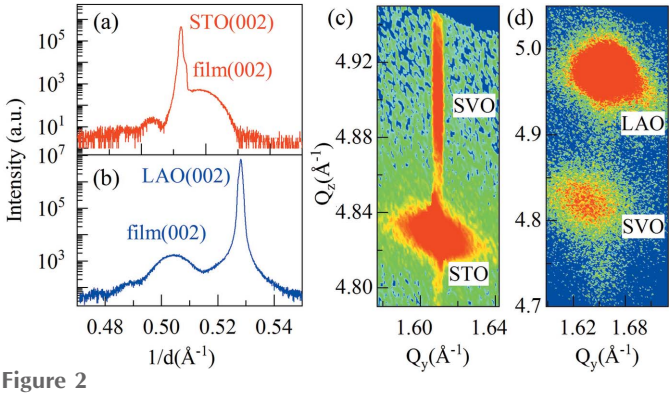

Figure 2
High resolution X-ray diffraction curves along the (002) direction for 26 u.c. $Sr_{1-y}VO_3$ thin films deposited on (*a*) an STO substrate and (*b*) an LAO substrate. (*c*) and (*d*) The corresponding reciprocal-space maps along the off-specular 013 reflection for $Sr_{1-y}VO_3$, respectively.

diffraction angles, the epitaxial films show average out-of-plane constants of 3.846 (8) and 3.94(2) Å for 26 u.c. $Sr_{1-y}VO_3$ deposited under tensile and compressive strains, respectively. The films deposited on STO are fully strained with the same in-plane lattice constant of 3.905 Å as the substrate. However, the 26 u.c. $Sr_{1-y}VO_3$ film deposited on compressively strained LAO is partially relaxed, *i.e.* with an in-plane lattice constant of 3.822 (5) Å compared with 3.79 Å for the LAO substrate. The relaxation R is defined to describe the strain state of $Sr_{1-y}VO_3$ thin films on STO and LAO as shown in Table 1, where $R = 0$ represents the fully strained state. We note that expansion of the out-of-plane lattice constant implies volume expansion of the deposited thin films, which might be related to octahedral tilts and the variation in the valence state for the transition metal ions, similar to what has been observed in ultrathin $La_{0.7}Sr_{0.3}MnO_3$ films (Sandiumenge *et al.*, 2013).

2.2. X-ray absorption measurements

Soft X-ray absorption measurements were performed on the 08U1A soft X-ray beamline at the Shanghai Synchrotron Radiation Facility, China. Data were obtained by collecting the photocurrent in total electron yield mode. All the absorption spectra presented here were subtracted with a linear background prior to the absorption edge, followed by normalization to the unit value at an energy above the absorption edges (*i.e.* $E \simeq 528.2$ eV).

The absorption spectra for 26 u.c. $Sr_{1-y}VO_3$ films are similar for both tensile and compressive strains in terms of the same excitation energies and spectral line shapes, as shown in Fig. 3. The spectra are composed of L_3 and L_2 sets of peaks owing to the spin–orbit coupling of the V 2*p* levels. A coexistence of V^{5+} and V^{4+} in thick $Sr_{1-y}VO_3$ films is suggested from: (i) the absorption energies, which are comparable with the reference spectrum of $Sr_2V_2O_7$ powder; and (ii) the existence of small fine structures around 516 eV as a feature only for V^{5+} but with less enhanced intensities. To give a further estimate of the amount of V^{5+} and V^{4+} contributing to the measured profiles, we fitted the absorption spectra using two Lorenztians. Since the absorption peak at the L_2-edge shows a broad peak feature for both V^{5+} and V^{4+}, we only consider the fit at the V L_3-edge, as shown in Figs. 3(*c*)–3(*d*). The fitting results of the spectral deconvolution are composed of two chemical states, where the low- and high-energy features arise from V^{4+} and V^{5+} chemical states, respectively. From the peak areas of the two Lorenztians, we estimate a mixture of 37% V^{5+} and 63% V^{4+} for the 26 u.c. $Sr_{1-y}VO_3$ film under tensile strain, whereas a mixture of 47% V^{5+} and 53% V^{4+} is obtained for the film under compressive strain. The amounts of V^{5+} and V^{4+} obtained from the fitting results suggest $y = 0.185$ considering charge conservation for the $Sr_{1-y}VO_3$ films under tensile strain, whereas $y = 0.235$ for the film under compressive strain.

Surprisingly, different thickness-dependent behaviours are observed for $Sr_{1-y}VO_3$films in different strain states. For $Sr_{1-y}VO_3$ films under tensile strain, the absorption spectrum of 5 u.c. shifts to low binding energies, *i.e.* the absorption edges lie ~0.7 eV lower in energy, as shown in Fig. 3(*a*). Note that the 10 u.c. $Sr_{1-y}VO_3$ thin film on an STO substrate already shows a small indication of a shift to lower energy. Lu *et al.* (2018) reported a systematic change in the V *L*-edge absorption spectra from V_2O_5 to VO_2 as a function of electric bias. Our absorption spectra of $Sr_{1-y}VO_3$ films show a comparable energy shift to low energy, suggesting a variation from a mixture of V^{5+} and V^{4+} in the 26 u.c. $Sr_{1-y}VO_3$ film to mainly V^{4+} in the 5 u.c. film. However, instead of a variation in the V valence state, we observe a change in the spectral line shape to narrow band features for $Sr_{1-y}VO_3$ films deposited on an LSAO substrate. The change in absorption spectral line shape lies at the same thickness, *i.e.* 10 u.c., as the critical thickness of $Sr_{1-y}VO_3$ films undergoing the metal-to-insulator transition shown in next section. This is similar to the change in the spectral line shape resolved in the thickness-dependent metal–

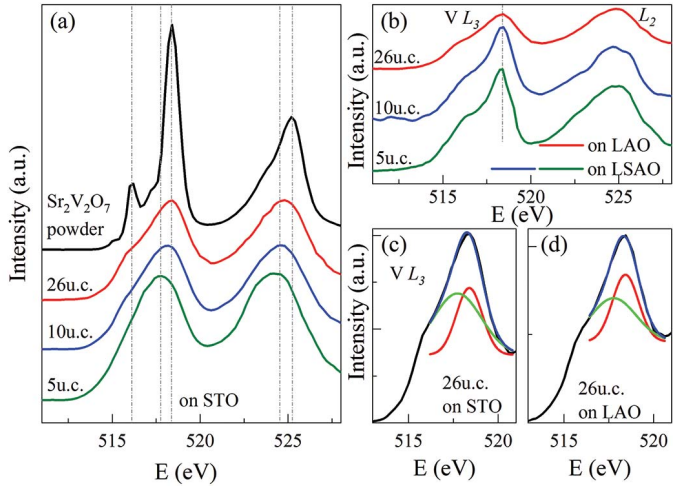

Figure 3
(*a*) The absorption spectra for $Sr_{1-y}VO_3$ films of different thicknesses from 26 to 5 u.c. on an STO substrate with tensile strain. A reference absorption spectrum from $Sr_2V_2O_7$ powder measured during the same beam time is shown for comparison. (*b*) The thickness-dependent absorption spectra for $Sr_{1-y}VO_3$ films of 26 u.c. on an LAO substrate, and 10 u.c. and 5 u.c. on LSAO substrates. The absorption spectra are shifted vertically by 2 for clarity. (*c*) and (*d*) The fitting results of the absorption spectra at the V L_3-edge for 26 u.c. $Sr_{1-y}VO_3$ films on an STO substrate with tensile strain and on LAO with a compressive strain, respectively.

insulator transition in rare earth nickelate thin films (Wu *et al.*, 2015).

2.3. DC transport measurements

Fig. 4 shows the temperature-dependent resistivity curves for $Sr_{1-y}VO_3$ thin films of different thicknesses and strains measured using the standard four-probe method. The $Sr_{1-y}VO_3$ film deposited on an STO substrate with tensile strain shows a metal–insulator transition at 5 u.c., whereas the compressive-strained $Sr_{1-y}VO_3$ film on an LSAO substrate shows an insulating behaviour at 10 u.c. For the metallic phase of $Sr_{1-y}VO_3$ with both tensile and compressive [Fig. 4(*a*)] strains, the resistivity curves deviate from a linear and temperature-dependent form related to the electron–phonon interaction (*i.e.* $\rho \propto T$). The temperature-dependent resistivity curves for metallic $Sr_{1-y}VO_3$ films are similar to the results reported for a $Ca_{1-x}Sr_xVO_3$ solid solution (Inoue *et al.*, 1998), SVO thin films (Gu *et al.*, 2014) and a system of SVO layers sandwiched by insulating $LaVO_3$ layers (Li *et al.*, 2015), which were understood through a T^2 dependence attributed to a strong electron–electron interaction up to room temperature. Similarly, the resistivity curves of our investigated $Sr_{1-y}VO_3$ films can be fitted well with $\rho \propto T^2$, as shown in Fig. 4(*a*).

Moreover, we note that the striking T^2 temperature-dependent resistivity behaviours (up to room temperature) are analogous to the results observed in the neighbouring doped titanates, where the transport behaviours were originally discussed in terms of strong electron–electron correlations, and then by the small polaronic conduction model (*e.g.* in $La_{2/3}TiO_3$ and $La_{1-y}TiO_{3+\delta}$ systems; Gariglio *et al.*, 2001; Jung *et al.*, 2000). Given the similar coexistence of $3d^0$ and $3d^1$ electronic configurations in cation-deficient $Sr_{1-y}VO_3$ films as in $La_{2/3}TiO_3$ and $La_{1-y}TiO_{3+\delta}$ systems, we tried to fit the resistivity curves using the small polaronic conduction model. Interestingly, the temperature-dependent resistivity relationship can be equally well fitted by a small polaronic transport, as shown in Fig. 4(*b*).

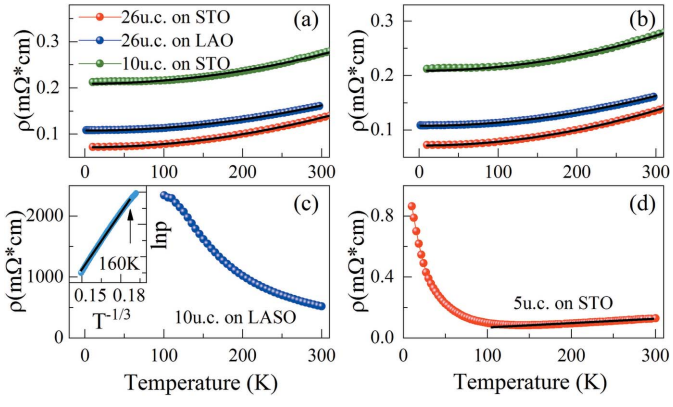

Figure 4
(*a*)–(*b*) Temperature-dependent resistivity curves for $Sr_{1-y}VO_3$ thin films of 26 u.c. on STO, 26 u.c. on LAO and 10 u.c. on STO substrates. The black lines in panel (*a*) show the fit with $\rho \propto T^2$ and those in panel (*b*) exhibit the fit with the small polaronic conduction model. (*c*) The ρ–T relationship for compressively strained $Sr_{1-y}VO_3$ films on LSAO. (*d*) The metal–insulator transition of 5 u.c. $Sr_{1-y}VO_3$ on an STO substrate.

The resistivity curves can be described by the following equation, considering only one low-lying optical mode ω_0 in the small polaronic conduction model (Gariglio *et al.*, 2001):

$$\rho(T) = \rho_0 + \frac{C}{\sinh^2(\hbar\omega_0/2k_BT)}, \quad (1)$$

with an identical value of $\hbar\omega_0/k_B$ = 80 K, where k_B is the Boltzmann constant. The other two parameters are: C = 0.00115 mΩ cm and ρ_0 = 0.072 mΩ cm for 26 u.c. $Sr_{1-y}VO_3$ on STO, C = 0.00115 mΩ cm and ρ_0 = 0.209 mΩ cm for 10 u.c. on STO, and C = 0.00098 mΩ cm and ρ_0 = 0.108 mΩ cm for 26 u.c. $Sr_{1-y}VO_3$ on an LAO substrate.

We note that the phonon frequency obtained from this fit has the same value as $\hbar\omega_0/k_B$ = 80 K resolved in doped $La_{1-y}TiO_{3+\delta}$ (Gariglio *et al.*, 2001) and doped $La_{1-x}Ca_xMnO_3$ systems (Zhao *et al.*, 2000), which suggests the existence of a soft mode related to the tilting/rotation of oxygen octahedra which is strongly coupled to the carriers (Zhao *et al.*, 2000). Further studies from either photoemission (Fujimori *et al.*, 1996) or optical spectroscopic measurements (Nucara *et al.*, 2008) would be useful to identify the optical phonon mode. However, the small polaron band which is expected to appear near the Fermi level in the photoemission measurements might be smeared out due to the broad valence band of V 3*d* states (Yoshimatsu *et al.*, 2011). Our thin films with thicknesses less than 26 u.c. and with 4 u.c. STO capping layers are challenging for optical measurements with typical in-house setups. It is therefore difficult to justify the intrinsic conducting mechanism here and it needs further investigation with different experimental designs.

Compared with the metallic behaviour of 10 u.c. $Sr_{1-y}VO_3$ films under tensile strain, the $Sr_{1-y}VO_3$ film of the same thickness on an LSAO substrate shows a strong insulating behaviour where the resistivity is beyond the measurement limit below 110 K, as shown in Fig. 4(*c*). This insulating behaviour cannot be fitted with either a thermally activated conduction model ($\ln\rho \propto 1/T$) or the activated hopping model of small polarons [$\ln(\rho/T) \propto 1/T$], which can instead be fitted reasonably well by a two-dimensional variable-range hopping (VRH) model [$\ln\rho \propto T^{-1/3}$, inset of Fig. 4(*c*)] and a three-dimensional VRH model ($\ln\rho \propto T^{-1/4}$) down to 160 K. The reasonable fitting of the resistivity curves using the VRH model suggests that the conduction model is governed by the localization of charge carriers and the hopping of carriers between different localized states. The localized bands are also visualized in the aforementioned X-ray absorption measurements. The resistivity measurement for 5 u.c. $Sr_{1-y}VO_3$ on an LSAO substrate is above the measurement limit at room temperature. The $Sr_{1-y}VO_3$ thin film with a thickness of 5 u.c exhibits a metal–insulator transition where the high-temperature regime shows a linear temperature dependence typical for metallic behaviour, *i.e.* $\rho \propto T$ shown as the black fit line in Fig. 4(*d*). The resistivity value of the 5 u.c. $Sr_{1-y}VO_3$ film on an STO substrate is lower than that of 10 u.c. $Sr_{1-y}VO_3$ on an STO substrate, which is opposite to the typical tendency

expected for reducing SVO film thicknesses (Gu *et al.*, 2014; Fouchet *et al.*, 2016). This might be related to the variation in stoichiometry, as suggested by the V L_2/L_3-edge absorption spectroscopy analysis with a change of V valence state in ultrathin 5 u.c. SVO films. The insulating regime is difficult to fit with the thermal or small polaronic activated conduction mechanism, or the VRH models.

2.4. EDX measurements

To investigate further for the presence of cation deficiencies, we provide local energy-dispersive X-ray (EDX) measurements for $Sr_{1-y}VO_3$ thin films deposited on different substrates, which probe the composition of individual elements in the thin films.

Fig. 5 displays the EDX spectra of $Sr_{1-y}VO_3$ thin films on (*a*) STO, (*b*) LAO and (*c*) LSAO substrates, while the corresponding atomic percentages of each individual element are listed in Table 2. Due to the existence of Sr in both the investigated thin films and the substrates such as STO and LSAO, the relative abundance of Sr content in the $Sr_{1-y}VO_3$ thin films can be roughly obtained by subtracting the atomic percentage of the substrate with an estimate of 1:1 for the substrates, *i.e.* Sr:Ti = 1:1 for the STO substrate and Sr:Al = 1:1 for the LSAO susbtrate. The atomic percentage of Sr in $Sr_{1-y}VO_3$ is denoted Sr_{subtr} after subtracting the contribution of the substrate. The ratios between Sr_{subtr} and V for each sample are shown in the last column of Table 2. The EDX measurements show the relative atomic deficiency of strontium for all the $Sr_{1-y}VO_3$ thin films under both compressive and tensile strains, which is consistent with the presence of Sr

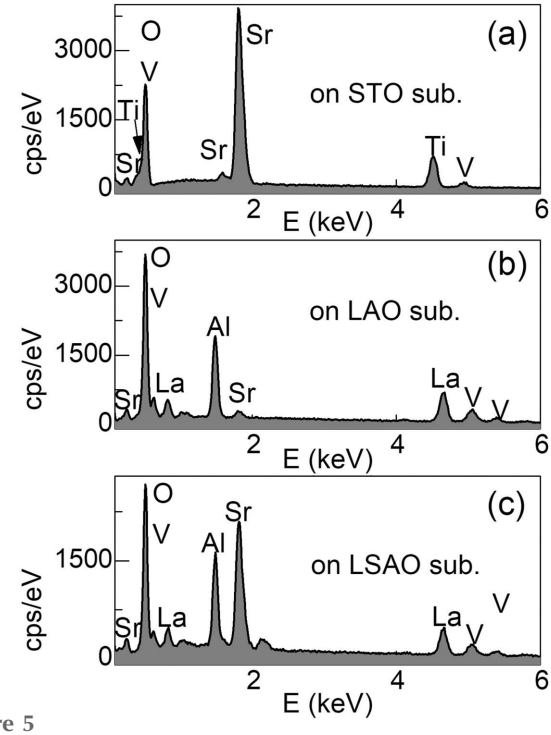

Figure 5
EDX spectra of $Sr_{1-y}VO_3$ thin films on (*a*) STO, (*b*) LAO and (*c*) LSAO substrates.

Table 2
The relative atomic percentages of individual elements for $Sr_{1-y}VO_3$ thin films deposited on different substrates.

For each sample, the EDX measurements were performed twice at different regions with a scanned area of ∼50 µm. The corresponding EDX spectra for the first measurement are shown in Fig. 5.

Substrate	O	Ti	V	Sr	Al	Sr_{subtr}:V
STO_{1st}	57.90	20.65	0.47	20.98		0.33:0.47
STO_{2nd}	58.22	20.65	0.74	20.78		0.53:0.74
LAO_{1st}	95.51		2.63	1.96		1.96:2.63
LAO_{2nd}	95.38		3.02	1.60		1.60:3.02
$LSAO_{1st}$	61.24		0.84	19.30	18.62	0.68:0.84
$LSAO_{2nd}$	61.50		0.46	19.12	18.92	0.2:0.46

deficiencies and the existence of V^{5+} in the investigated thin films as discussed above.

3. Discussion and conclusions

In contrast with the existence of oxygen vacancies expressed in the form $ABO_{3-\delta}$ in perovskite oxides, the perovskite structure is close-packed in terms of its large oxygen anion backbone structure which is unlikely to leave additional room for oxygen interstitials. Charge-sensitive X-ray absorption measurements at the V *L*-edge show the coexistence of V^{5+} and V^{4+} in our investigated $Sr_{1-y}VO_3$ films. Creating cation deficiencies is required to compensate the V^{5+} valence state from the stoichiometric point of view.

In cation-deficient $Sr_{1-y}VO_3$ thin films capped with 4 u.c. STO layers, we observe different responses of the stoichiometric environment to epitaxial strains in ultrathin films, *i.e.* a variation in the V chemical valence state is only resolved for $Sr_{1-y}VO_3$ ultrathin films under tensile strain. Similar to the usage of the formation energy of oxygen vacancies (ΔE_{vac}) in understanding the relationship between strain and oxygen vacancies in many perovskite compounds, we use the formation energy of cation deficiencies to describe our results. Our results indicate a larger cation-deficient formation energy for $Sr_{1-y}VO_3$ ultrathin films under tensile strain. This is opposite to the decrease in ΔE_{vac} as the magnitude of the tensile strain increases. We further note that the interaction between elastic strain and ΔE_{vac} is nontrivial (Herklotz *et al.*, 2017), *i.e.* both a linear reduction in ΔE_{vac} as the strain increases (Marrocchelli *et al.*, 2015) and a nearly quadratic dependence (Choi *et al.*, 2015; Iglesias *et al.*, 2017) have been proposed. Therefore, the observed asymmetric response of the cation-deficiency formation energy to elastic strain deserves further detailed theoretical calculations.

The resistivity curves of metallic $Sr_{1-y}VO_3$ films clearly deviate from a linear temperature dependence, which can be understood by a T^2 dependence attributed to strong electron–electron correlations as reported previously. However, the resistivity curves can be fitted equally well by a small polaronic transport mechanism. The small polaronic conduction model as the dominant scattering mechanism has been proposed in doped titanates (Gariglio *et al.*, 2001; Jung *et al.*, 2000) involving the coexistence of $3d^0$ and $3d^1$ electronic configurations,

which is exactly the same situation as the $Sr_{1-y}VO_3$ films investigated here. Our studies draw attention to the electron–phonon interaction as a possible dominant mechanism for transport behaviour.

Furthermore, the $Sr_{1-y}VO_3$ films undergo metal–insulator transitions at different critical thicknesses under different strains. The strain-dependent response of electrical resistivity varies in different systems as reported in the literature. Taking nickel oxide thin films as an example, although asymmetric responses of electrical resistivity to compressive and tensile strains were reported in 12 nm $PrNiO_3$ films (Hepting *et al.*, 2014) and in 6 nm $NdNiO_3$ films (Mundet *et al.*, 2018), symmetric responses to compressive and tensile strains were also observed in several thin-film systems. For instance, the low-temperature upturn in the resistivity curves for both tensile and compressive strained cases can be described by the same model for 6 nm $LaNiO_3$ films (Moon *et al.*, 2011). The metal–insulator transition temperatures change with different magnitudes for tensile and compressive strains, but the low-temperature region of the resistivity curves could in all cases be fitted with the VRH model in 60 nm $PrNiO_3$ films (Dan *et al.*, 2016) and in 12 nm $NdNiO_3$ films (Xiang *et al.*, 2013). The asymmetric response of electrical conductivity to strain in $Sr_{1-y}VO_3$ ultrathin films, in particular for the 5 u.c. $Sr_{1-y}VO_3$ film under tensile strain, might be related to the variation in V valence states as resolved from the V L_2/L_3-edge absorption measurements.

The strain-induced tuning of the Sr/V ratio offers guidance for thin-film synthesis in other multivalent compounds. The asymmetric response of the electrical conductivity and cation-deficiency formation energy to epitaxial tensile and compressive strain are beneficial to understand the defect chemistry of functional oxide electronic devices, to investigate the novel physical properties arising from interfacial charge transfer in thin films and heterostructures, and to engineer potential electronic applications.

Acknowledgements

We acknowledge the provision of synchrotron radiation beamtime and the support given by L. J. Zhang at the Shanghai Synchrotron Radiation Facility.

Funding information

Funding for this research was provided by: National Natural Science Foundation of China (grant No. 11704317); China Postdoctoral Science Foundation (grant No. 2016M602064); Fundamental Research Funds for Central Universities (grant No. 20720160020).

References

Cao, Y., Liu, X., Kareev, M., Choudhury, D., Middey, S., Meyers, D., Kim, J.-W., Ryan, P. J., Freeland, J. & Chakhalian, J. (2016). *Nat. Commun.* **7**, 10418.

Choi, S.-Y., Kim, S.-D., Choi, M., Lee, H.-S., Ryu, J., Shibata, N., Mizoguchi, T., Tochigi, E., Yamamoto, T., Kang, S.-J. L. & Ikuhara, Y. (2015). *Nano Lett.* **15**, 4129–4134.

Farokhipoor, S. & Noheda, B. (2011). *Phys. Rev. Lett.* **107**, 127601.

Fouchet, A., Allain, M., Bérini, B., Popova, E., Janolin, P.-E., Guiblin, N., Chikoidze, E., Scola, J., Hrabovsky, D., Dumont, Y. & Keller, N. (2016). *Mater. Sci. Eng. B*, **212**, 7–13.

Fujimori, A., Bocquet, A. E., Morikawa, K., Kobayashi, K., Saitoh, T., Tokura, Y., Hase, I. & Onoda, M. (1996). *J. Phys. Chem. Solids*, **57**, 1379–1384.

Gariglio, S., Seo, J. W., Fompeyrine, J., Locquet, J.-P. & Triscone, J.-M. (2001). *Phys. Rev. B*, **63**, 161103.

Gu, M., Wolf, S. A. & Lu, J. (2014). *Adv. Mater. Interfaces*, **1**, 1300126.

Hepting, M., Minola, M., Frano, A., Cristiani, G., Logvenov, G., Schierle, E., Wu, M., Bluschke, M., Weschke, E., Habermeier, H.-U., Benckiser, E., Le Tacon, M. & Keimer, B. (2014). *Phys. Rev. Lett.* **113**, 227206.

Herklotz, A., Lee, D., Guo, E.-J., Meyer, T. L., Petrie, J. R. & Lee, H. N. (2017). *J. Phys. Condens. Matter*, **29**, 493001.

Iglesias, L., Sarantopoulos, A., Magén, C. & Rivadulla, F. (2017). *Phys. Rev. B*, **95**, 165138.

Inoue, I. H., Goto, O., Makino, H., Hussey, N. E. & Ishikawa, M. (1998). *Phys. Rev. B*, **58**, 4372–4383.

Jung, W. H., Wakai, H., Nakatsugawa, H. & Iguchi, E. (2000). *J. Appl. Phys.* **88**, 2560–2563.

Li, Q.-R., Major, M., Yazdi, M. B., Donner, W., Dao, V. H., Mercey, B. & Lüders, U. (2015). *Phys. Rev. B*, **91**, 035420.

Lu, Q., Bishop, S. R., Lee, D., Lee, S., Bluhm, H., Tuller, H. L., Lee, H. N. & Yildiz, B. (2018). *Adv. Funct. Mater.* **28**, 1803024.

Ma, J., Zhang, Y., Wu, L., Song, C., Zhang, Q., Zhang, J., Ma, J. & Nan, C.-W. (2016). *MRS Commun.* **6**, 354–359.

Marrocchelli, D., Sun, L. & Yildiz, B. (2015). *J. Am. Chem. Soc.* **137**, 4735–4748.

Mirjolet, M., Sánchez, F. & Fontcuberta, J. (2019). *Adv. Funct. Mater.* **29**, 1808432.

Moon, E. J., Gray, B. A., Kareev, M., Liu, J., Altendorf, S. G., Strigari, F., Tjeng, L. H., Freeland, J. W. & Chakhalian, J. (2011). *New J. Phys.* **13**, 073037.

Moyer, J. A., Eaton, C. & Engel-Herbert, R. (2013). *Adv. Mater.* **25**, 3578–3582.

Mundet, B., Jareño, J., Gazquez, J., Varela, M., Obradors, X. & Puig, T. (2018). *Phys. Rev. Mater.* **2**, 063607.

Nucara, A., Maselli, P., Del Bufalo, M., Guidi, M. C., Garcia, J., Orgiani, P., Maritato, L. & Calvani, P. (2008). *Phys. Rev. B*, **77**, 064431.

Ohtomo, A., Muller, D. A., Grazul, J. L. & Hwang, H. Y. (2002). *Appl. Phys. Lett.* **80**, 3922–3924.

Pan, S. H., O'Neal, J. P., Badzey, R. L., Chamon, C., Ding, H., Engelbrecht, J. R., Wang, Z., Eisaki, H., Uchida, S., Gupta, A. K., Ng, K.-W., Hudson, E. W., Lang, K. M. & Davis, J. C. (2001). *Nature*, **413**, 282–285.

Sandiumenge, F., Santiso, J., Balcells, L., Konstantinovic, Z., Roqueta, J., Pomar, A., Espinós, J. P. & Martínez, B. (2013). *Phys. Rev. Lett.* **110**, 107206.

Sawa, H., Ninomiya, E., Ohama, T., Nakao, H., Ohwada, K. J., Murakami, Y., Fujii, Y., Noda, Y., Isobe, M. & Ueda, Y. (2002). *J. Phys. Soc. Jpn*, **71**, 385–388.

Skjaervø, S. H., Wefring, E. T., Nesdal, S. K., Gaukås, N. H., Olsen, G. H., Glaum, J., Tybell, T. & Selbach, S. M. (2016). *Nat. Commun.* **7**, 13745.

Stemmer, S., Jacobson, A. J., Chen, X. & Ignatiev, A. (2001). *J. Appl. Phys.* **90**, 3319–3324.

Tarun, M. C., Selim, F. A. & McCluskey, M. D. (2013). *Phys. Rev. Lett.* **111**, 187403.

Wang, J., Rijnders, G. & Koster, G. (2018). *Appl. Phys. Lett.* **113**, 223103.

Wu, M., Benckiser, E., Audehm, P., Goering, E., Wochner, P., Christiani, G., Logvenov, G., Habermeier, H.-U. & Keimer, B. (2015). *Phys. Rev. B*, **91**, 195130.

Wu, M., Zheng, J.-C. & Wang, H.-Q. (2018). *Phys. Rev. B*, **97**, 245138.
Xiang, P.-H., Zhong, N., Duan, C.-G., Tang, X. D., Hu, Z. G., Yang, P. X., Zhu, Z. Q. & Chu, J. H. (2013). *J. Appl. Phys.* **114**, 243713.
Yao, D., Shi, L., Zhou, S., Liu, H., Wang, Y., Zhao, J. & Li, Y. (2016). *J. Phys. D Appl. Phys.* **49**, 125301.
Yoshimatsu, K., Horiba, K., Kumigashira, H., Yoshida, T., Fujimori, A. & Oshima, M. (2011). *Science*, **333**, 319–322.
Yoshimatsu, K., Sakai, E., Kobayashi, M., Horiba, K., Yoshida, T., Fujimori, A., Oshima, M. & Kumigashira, H. (2013). *Phys. Rev. B*, **88**, 115308.
Yoshino, T., Okawa, M., Kajita, T., Dash, S., Shimoyama, R., Takahashi, K., Takahashi, Y., Takayanagi, R., Saitoh, T., Ootsuki, D., Yoshida, T., Ikenaga, E., Saini, N. L., Katsufuji, T. & Mizokawa, T. (2017). *Phys. Rev. B*, **95**, 075151.
Zhao, G., Smolyaninova, V., Prellier, W. & Keller, H. (2000). *Phys. Rev. Lett.* **84**, 6086–6089.